Real-Time Elimination of Specular Reflectance in Color Images by 2D Histogram and Mathematical Morphology

Francisco Ortiz†, Fernando Torres and Francisco Candelas
Automatics, Robotics and Computer Vision Group., Dept. Physics, Systems Engineering and Signal Theory, University of Alicante, Alicante, SPAIN

This article proposes a real-time method for the detection and elimination of specular reflectance in color images. We use a 2D histogram that allows us to relate the signals of luminance and saturation of a color image and to identify the specularities in a given area of the histogram. This is known as the LS diagram and it is constructed from the HLS color space. A detailed study of the presence of specularities in the diagram for different types of materials is carried out. To eliminate the specularities detected, we use a new connected vectorial filter based on color morphology and adapted to real-time specifications. This filter operates only in the bright zones previously detected, reducing the high cost of processing of connected filters and avoiding over-simplification, in single processing and multiprocessing environments. The new proposed method achieves good and similar results to the ones obtained with other techniques used in multimedia, but it not requires costly multiple-view systems or stereo images.

Journal of Imaging Science and Technology 49: 220–229 (2005)

Introduction

Real-time image processing differs from "ordinary" image processing in that the same correct results must be obtained in critical time. Real-time imaging covers a multidisciplinary range of research areas including image compression, image enhancement and filtering, visual inspection, etc.[1] Indeed, a goal in computer vision is to identify objects of real scenes in the shortest time possible or within a deadline. Sometimes, this goal is not easy since bad adjustment of illumination can introduce brightness (highlights or specular reflectance) in the objects captured by the vision system. The presence of brightness causes problems in low level computer vision methods such as segmentation (which typically assumes uniform or smoothly varying intensity across a surface), stereo or motion analysis (which attempt to match images taken from different viewpoints) and in high level operations such as multimedia applications, where the brightness affects the visual quality of the scene.

To be able to eliminate the highlights in captured scenes, we must identify them first. The dichromatic reflection model proposed by Safer[2] is a tool that has been used in many methods for detecting specularities. This model supposes that the interaction between the light and a dielectric material produces different spectral distributions in the object, i.e., the specular and diffuse reflectances. The specular reflectance has the same spectral makeup as the incident light whereas the diffuse component is a product of illumination and surface pigments. Based on this model, Lin et al[3] have developed a system for eliminating specularities in image sequences by means of stereo correspondence. Bajcsy et al[4] use a chromatic space based on polar coordinates that allows the detection of specular and diffuse reflections by means of the previous knowledge of the captured scene. Klinker et al[5] employ a pixel clustering algorithm which has been shown to work well in detecting brightness in images of plastic objects. These previous approaches have produced good results but they have requirements that limit their applicability, such as the use of stereo or multiple-view systems, high time of processing, the previous knowledge of the scene, or the assumption of a homogeneous illumination, without considering the inter-reflections present in most typical real scenes.

In this article we explain a new and real-time system for the detection and elimination of brightness in color images by means of two main steps:

- *Detection*: we use a 2D histogram of luminance and saturation signals from a 3D polar coordinate color representation. This new representation allows us to obtain a specular reflectance map of the image.
- *Elimination*: we develop a vectorial geodesic reconstruction algorithm, which has low cost and avoids the over-simplification of the image.

Original manuscript received July 16, 2004

†Corresponding Author: F. Ortiz, fortiz@ua.es

Supplemental Material—Figures 3, 9, and 10 can be found in color on the IS&T website (www.imaging.org) for a period of no less than two years from the date of publication.

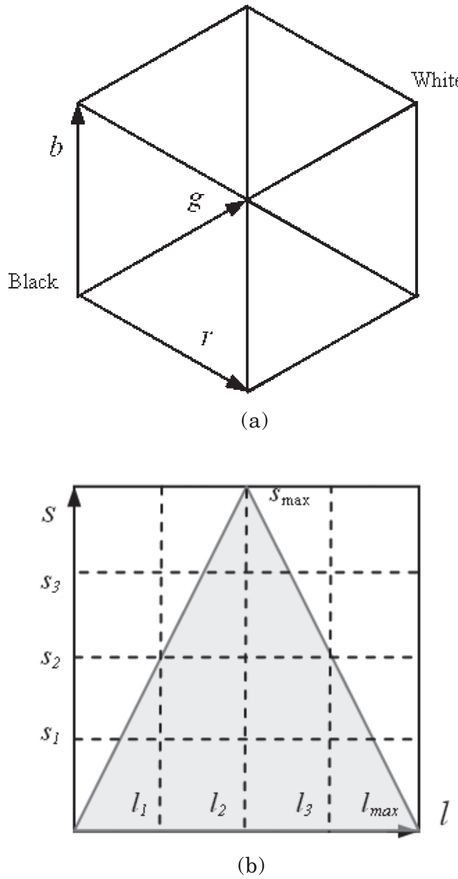

Figure 1. RGB cube and 2D positive histogram (a) 3D RGB cube; and (b) 2D positive LS diagram, $l_1 = 64$, $l_2 = 127$, $l_3 = 191$, $l_{max} = 255$, $s_1 = 64$, $s_2 = 127$, $s_3 = 191$, $s_{max} = 255$.

Color Spaces for Processing and LS Diagram

In recent years, the color spaces based in polar coordinates (HLS, HSV, HSI…) have been widely used in image processing.[6-8] Important advantages of these color spaces are: good compatibily with human intuition of colors and separability of chromatic values from achromatic values. One of most popular of these color models is the HLS (hue, luminance and saturation) and like other intuitive color spaces, the HLS is derived from the RGB cube (Fig. 1(a)), where the luminance and saturation values are calculated as follows:

$$\begin{cases} l = \dfrac{\max(r,g,b)+\min(r,g,b)}{2} \\ s = \begin{cases} \dfrac{\max(r,g,b)-\min(r,g,b)}{\max(r,g,b)+\min(r,g,b)} & if\ l \leq 0.5 \\ \dfrac{\max(r,g,b)-\min(r,g,b)}{2-\max(r,g,b)+\min(r,g,b)} & if\ l > 0.5 \end{cases} \end{cases} \qquad (1)$$

where *r, g, b, s* and *l* range from 0 to 1.

The HLS representation has a cylindrical shape according to the previous formulas. Some instability arises, however, in saturation for small variations of RGB values. To avoid this, we must linearly reduce the saturation as the luminance increases or decreases. This way, we change from a cylindrical geometrical representation to a double cone shape. The saturation map is now more amenable to image processing.[9]

We propose to exploit the existing relation of the specularities presents in a color image with specific coordinates of l and s, independently of the hue of the object in which the brightness appears.[10] Figure 1b shows the LS diagram as the positive projection of all of the corners of the RGB cube in a normalization of the achromatic line to l signal and where l and s now range from 0 to 255. The diagram is divided in 16 homogenous regions that segment pixels of a chromatic image by different thresholds of luminance and saturation. The LS diagram is a grey image $f(l,s)$ in which each coordinate (l,s) indicates the quantity of the pixels in values of luminance and saturation of the original color image.

Color Mathematical Morphology

The definition of morphological operators needs a totally ordered complete lattice structure.[11] The color pixels do not present, a priori, this structure and it is necessary to impose an order relationship in the color spaces. Several studies have been carried out on the application of mathematical morphology to color images.[9,12–15] The approach most commonly adopted is based on the use of a lexicographical order, which imposes total order on the color vectors. This way, we avoid the false colors in an individual filtering of signals. Let $\mathbf{x} = (x_1, x_2, .., x_n)$ and $\mathbf{y} = (y_1, y_2, \ldots, y_n)$ be two arbitrary vectors ($\mathbf{x,y} \in Z^n$). An example of lexicographical order o_{lex}, will be:

$$\mathbf{x} < \mathbf{y} \ \text{ if } \begin{cases} x_1 < y_1 \ \text{ or} \\ x_1 = y_1 \ \text{ and } \ x_2 < y_2 \ \text{ or} \\ x_1 = y_1 \ \text{ and } \ x_2 = y_2 \ldots \ \text{and} \ldots x_n < y_n \end{cases} \qquad (2)$$

On the other hand, it is important to define the color space in which operations are to be made. We use a color space based in attributes of luminance, saturation and hue. The preference of the components of the HLS model in the lexicographical ordering depends on the application and the properties of the image. Ordering with luminance in the first position is the best way of preserving the contours of the objects in the image (lattice influenced by luminance). For our application, we employ this strategy and we define a lattice with a lexicographical order of o_{lex} = luminance→saturation→hue.[9,13] Thus, we put more emphasis on the luminance signal. Afterwards, we analyze the saturation. Next, we compare a hue distance value, only if the pixels are colored and they have same intensity and saturation.

Vector Connected Filters

Morphological filters by reconstruction have the property of suppressing details, and preserving the contours of the remaining objects.[16–18] The use of these filters in color images requires an order relationship among the pixels of the image. For the vectorial morphological processing, the lexicographical ordering, previously defined o_{lex}, will be used. As such, the infimum ($\wedge_v$) and supremum ($\vee_v$) will be vectorial operators, and they will select pixels according to the order o_{lex} in the HLS color space.

Once the orders have been defined, the morphological operators of reconstruction for color images can be generated and applied. An elementary geodesic operation is the geodesic dilation. Let $\boldsymbol{g}$ denote a marker color image and $\boldsymbol{f}$ a mask color image (if $o_{lex}(\boldsymbol{g}) \leq o_{lex}(\boldsymbol{f})$, then $(\boldsymbol{g}) \wedge_v \boldsymbol{f} = \boldsymbol{g}$). The vectorial geodesic dilation of size 1 of the marker image $\boldsymbol{g}$ with respect to the mask $\boldsymbol{f}$ can be defined as:

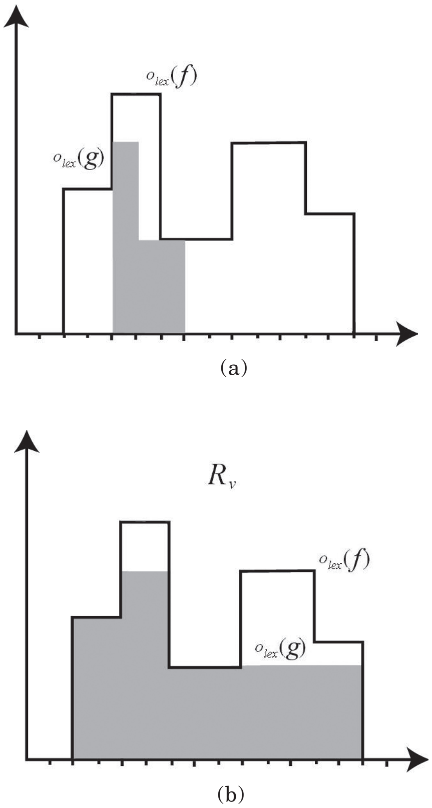

Figure 2. Vectorial reconstruction by dilation of a mask image $\boldsymbol{f}$ from a marker colour image $\boldsymbol{g}$. (a) Lexicographical ordering of vector signals $\boldsymbol{f}$ and $\boldsymbol{g}$; and (b) Result of the connected filter.

$$\delta_{v_{\boldsymbol{f}}}^{(1)}(\boldsymbol{g}) = \delta_{v}^{(1)}(\boldsymbol{g}) \wedge_{v} \boldsymbol{f} \tag{3}$$

where $\delta_{v}^{(1)}{}_{(\boldsymbol{g})}$ is the vectorial dilation of size 1 of the marker image $\boldsymbol{g}$. This propagation is limited by the mask $\boldsymbol{f}$.

The vectorial geodesic dilation of size n of a marker color image $\boldsymbol{g}$ with respect to a mask color image $\boldsymbol{f}$ is obtained by performing n successive geodesic dilations of $\boldsymbol{g}$ with respect to $\boldsymbol{f}$:

$$\delta_{v_{\boldsymbol{f}}}^{(n)}(\boldsymbol{g}) = \delta_{v_{\boldsymbol{f}}}^{(1)}\left[\delta_{v_{\boldsymbol{f}}}^{(n-1)}(\boldsymbol{g})\right] \tag{4}$$

with

$$\delta_{v_{\boldsymbol{f}}}^{(0)}(\boldsymbol{g}) = \boldsymbol{f}\,.$$

Geodesic transformations of images always converge after a finite number of iterations. The propagation of the marker image is limited by the mask image. Morphological reconstruction of a mask image is based on this principle.

The vectorial reconstruction by dilation of a mask color image $\boldsymbol{f}$ from a marker color image $\boldsymbol{g}$, (both with $D_f = D_g$ and $o_{\text{lex}}(\boldsymbol{g}) \le o_{\text{lex}}(\boldsymbol{f})$) can be defined as:

$$R_{v_{\boldsymbol{f}}}(\boldsymbol{g}) = \delta_{v_{\boldsymbol{f}}}^{(n)}(\boldsymbol{g}) \tag{5}$$

where n is such that

$$\delta_{v_{\boldsymbol{f}}}^{(n)}(\boldsymbol{g}) = \delta_{v_{\boldsymbol{f}}}^{(n+1)}(\boldsymbol{g})\,.$$

In Fig. 2, we can see an example of vectorial reconstruction of signals by means of a lexicographical order.

Actually, the high computational cost of processing of the connected vectorial filters precludes application of these operations in real-time algorithms. For this reason, these filters are recommended only for high level applications. In this article we will use the filters by reconstruction in low level tasks by means of a controlled filtering in specific areas of previously segmented images. This will permit us to achieve real-time requirements in image analysis.

Algorithm for Detecting and Eliminating Specularities

It is known that the specularities in the chromatic image have values of high luminance and low saturation. In Ref. 19, Androutsos et al. produce a division of the luminance-saturation space and they conclude that if the saturation is greater than 20% and the luminance is greater than 75%, the pixels are chromatic, if the saturation is smaller than 20% and the luminance is greater than 75%, the pixels are luminous or highlights. Our criterion is similar and it is based on the division of the luminance-saturation space into 16 homogenous regions that segment the chromatic image. The exact limits of the regions must be calculated, and one aim of this article is to specify these values.

The achromatic axes zone could be considered as a highlight. This is partly true because it is only fulfilled for grayscale images. In the HLS color space, as luminance l decreases, the brightness shows an increasingly similar surface color (diffuse reflection) for the objects on which this brightness appears, approaching the $s_{\max}$ value, defined as follows:

$$s_{\max} = \begin{cases} 2l & \text{if } l \in [0,\ 127] \\ -2(l-255) & \text{if } l \in [128,\ 255] \end{cases} \tag{6}$$

where $l \in [0, 255]$, $s \in [0, 255]$.

Contrast Enhancement by Color Morphology

An important consideration is that not all the images have the same dynamic range and, therefore, the values of luminance and saturation of their specularities do not correspond with the positions of the LS diagram previously presented. The above mentioned problem could be solved with a contrast enhancement by histogram equalization. Nevertheless, the histogram equalization of the original image can cause excessive increase of luminance, over-saturation and false detection of brightness. The best solution is to apply a new vector morphological contrast enhancement for luminous pixels, which considers the local features of the images. Specifically, the white top hat operator is added to the original image to enhance bright objects.[20] We denote the color morphological contrast enhancement by:

$$\boldsymbol{f}' = \boldsymbol{f} + WTH_{v}(\boldsymbol{f}) \tag{7}$$

where $\boldsymbol{f}'$ is the new contrasted color image and $WTH_v(\boldsymbol{f})$ is the vectorial top hat ($\boldsymbol{f}$-$\gamma_v(\boldsymbol{f})$) of the original color image $\boldsymbol{f}$. The color morphological contrast enhancement expels only the highlights to the limits of the RGB cube.

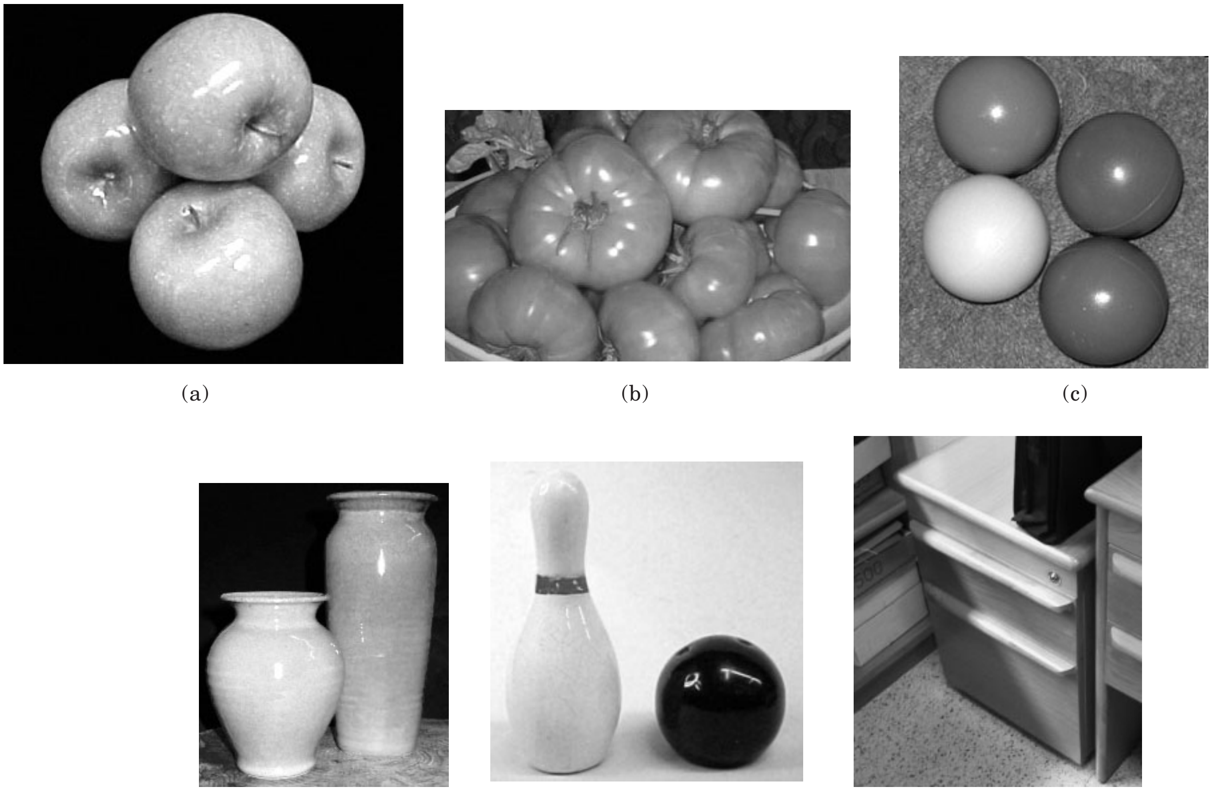

(a) (b) (c) (d) (e) (f)

Figure 3. Color images for empirical study. Different types of materials: Fruits in (a) “Apples”; (b) “Tomatoes”; (c) Plastics in “Balloons”; (d) “Bowling”; (e) Ceramics in “Vases”; and (f) Wood in “Drawers”. *Supplemental Material—Figure 3 can be found in color on the IS&T website (www.imaging.org) for a period of no less than two years from the date of publication.*

Highlight Detection

After color image contrast enhancement, the pixels of specular reflectance are positioned on the s_{max} line with high values of l. All the specularities are identified along the coordinates of the s_{max} line, from $s = 0$ to a threshold of s defined by s_{sp}. We present the results of a study for highlight detection carried out on a set of real chromatic images that are quite representative of countless common materials, i.e., plastic, ceramics, fruit, wood, etc., in which there are strong and weak reflectances. A subset of the images used in the study is presented in Fig. 3. The LS diagrams of these images are shown in Fig. 4. As can be seen, the maximum values of s along l are limited to the shape of LS-diagram of Fig. 1(b).

First, we select pixels of color image which are located on s_{max} line in region defined by $[l_3 - l_{max}, 0 - s_1]$ of LS diagram (Fig. 1(b)). As can be seen in Fig. 5, all of the specularities have been detected in this region and there is no presence of false brightness.

Figure 6 shows the evolution of the specularities detected when saturation is increased along s_{max}. It is a logarithmic evolution where most of the bright pixels are located as maximum values of luminance and minimum values of saturation. The rest correspond to the transition from specular to diffuse reflection of the dichromatic reflection model[2] on the surfaces of the objects.

The graphs show that the detection of specularities stops in all of the images for a threshold of s smaller than s_3, concretely, 10% of maximum saturation ($s_{sp} = 25$), and at higher values, no additional pixels in the image are detected as brightness. It is now easy to calculate the value of l_{sp} in HLS from Eq. (6), as:

$$l_{sp} = \frac{-s_{sp} + 510}{2} \tag{8}$$

Highlight Elimination

To eliminate the highlight that was previously detected with the LS diagram, we use a real-time geodesic filter. It is a vectorial opening by reconstruction applied only in the specular areas of the image and their surroundings. In this case, a new mask image h represents the pixels of $\boldsymbol{f}$ with which we will be operating. The mask image h is a dilation of size e of the mask of specularities (Fig. 5). Assuming that $D_h = D_f$, each pixel (x,y) has a value of $h(x,y) = \{0,1\}$, where $h(x,y) = 1$ in the new areas of interest in the image. The size e of the structural element of the dilation will determine the success of the reconstruction and the final cost of the operations, since this size imposes the process area of the filters.

In the geodesic filter, $\boldsymbol{f}$ is first eroded. The eroded sets are then used as sets for a reconstruction of the original image. The new filter is defined, taking into account the fact that, in this case, the operation will not affect all the pixels (x,y), but only those in which $h(x,y) = 1$:

$$\gamma_{v\boldsymbol{f},h}^{(n')} = \left\{ \delta_{v\boldsymbol{f}}^{(n')}(\varepsilon_v^{(e)}(\boldsymbol{f})) \;\;|\;\; \forall \boldsymbol{f}(x,y) \Rightarrow h(x,y) = 1 \right\} \tag{9}$$

where n' is such that

$$\delta_{v\boldsymbol{f}}^{(n')}(\varepsilon_v^{(e)}(\boldsymbol{f})) = \delta_{v\boldsymbol{f}}^{(n'+1)}(\varepsilon_v^{(e)}(\boldsymbol{f})).$$

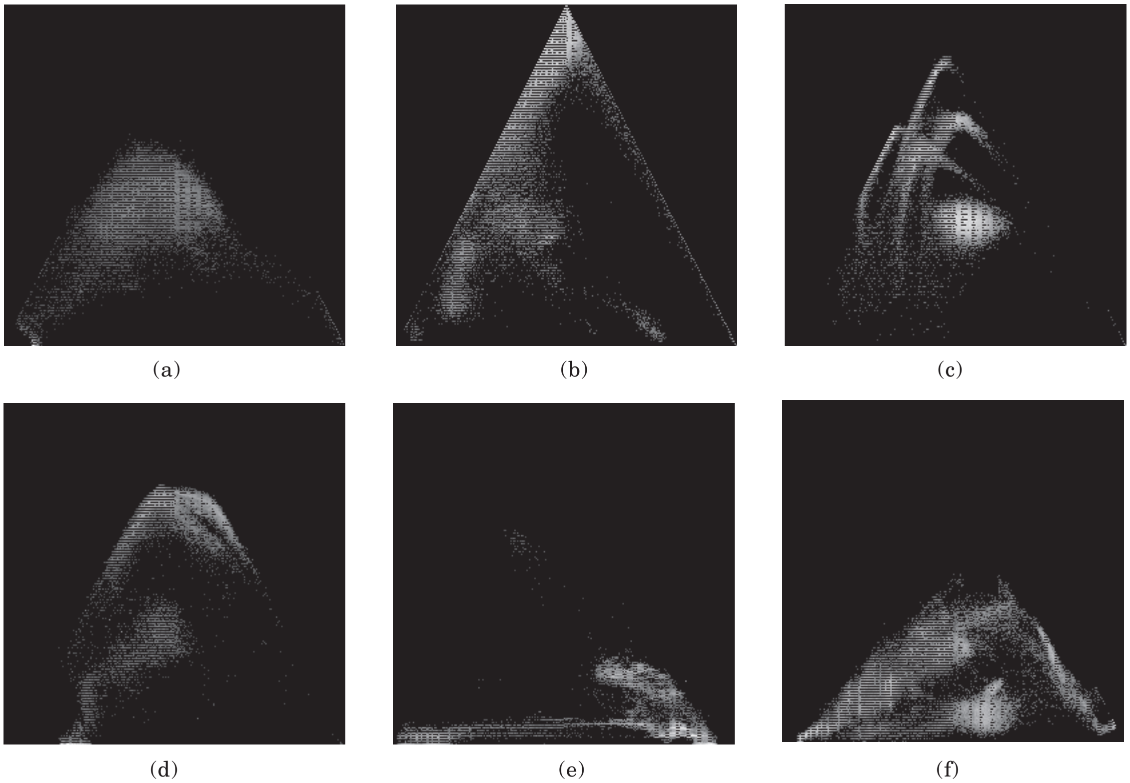

Figure 4. LS diagram of contrasted color images from Fig. 2.

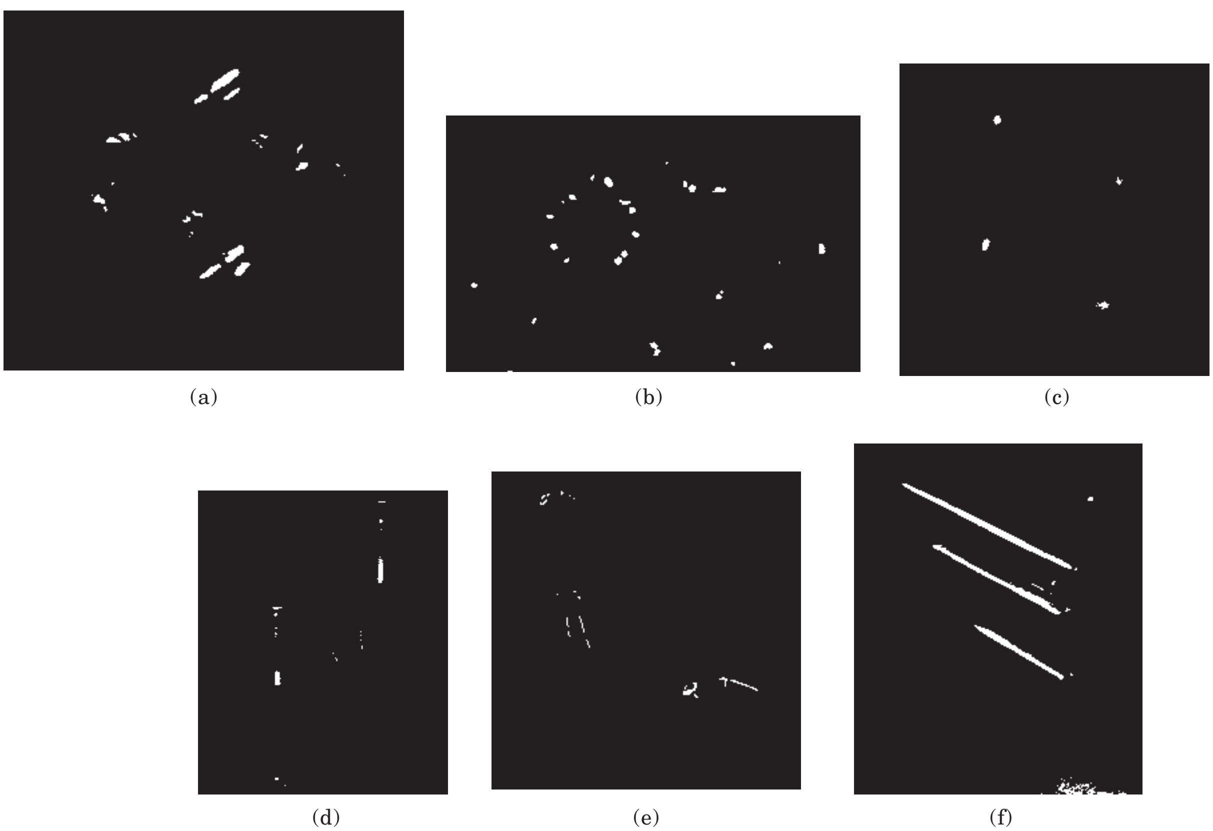

Figure 5. Masks of brightness. Experimental results for original images in Fig. 2: (a) bright pixels: 617 in 300 × 270 of "Apples"; (b) 889 in 330 × 204 of "Tomatoes"; (c) 104 in 232 × 234 of "Balloons"; (d) 143 in 208 × 253 of "Vases"; (e) 176 in 223 × 229 of "Bowling"; and (f) 1465 in 216 × 263 of "Drawers".

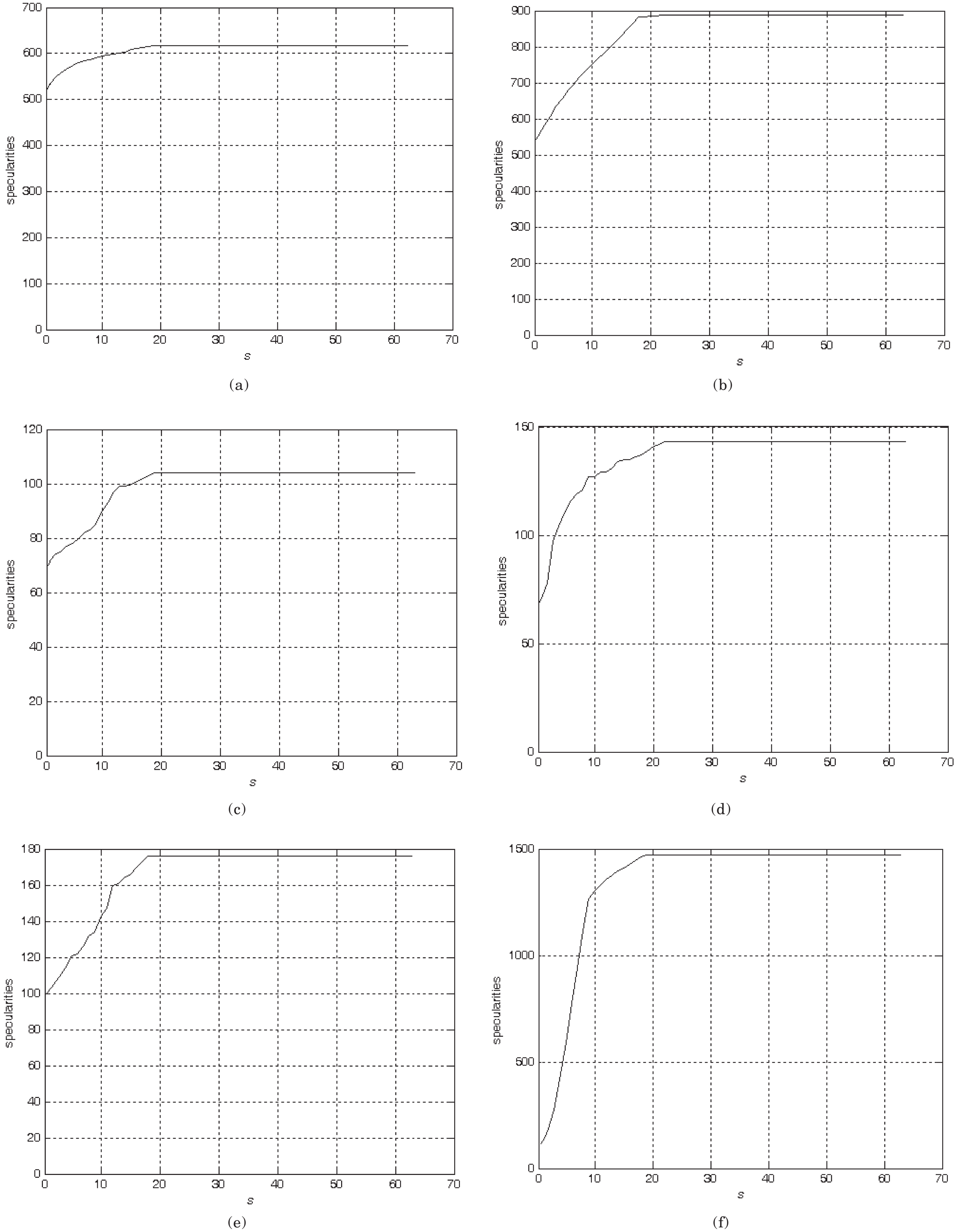

Figure 6. Evolution of the specularities detected according to values of s by s_{max} line in LS diagram: (a) “Apples”; (b) “Tomatoes”; (c) “Balloons”; (d) “Vases”; (e) “Bowling”; and (f) “Drawers”.

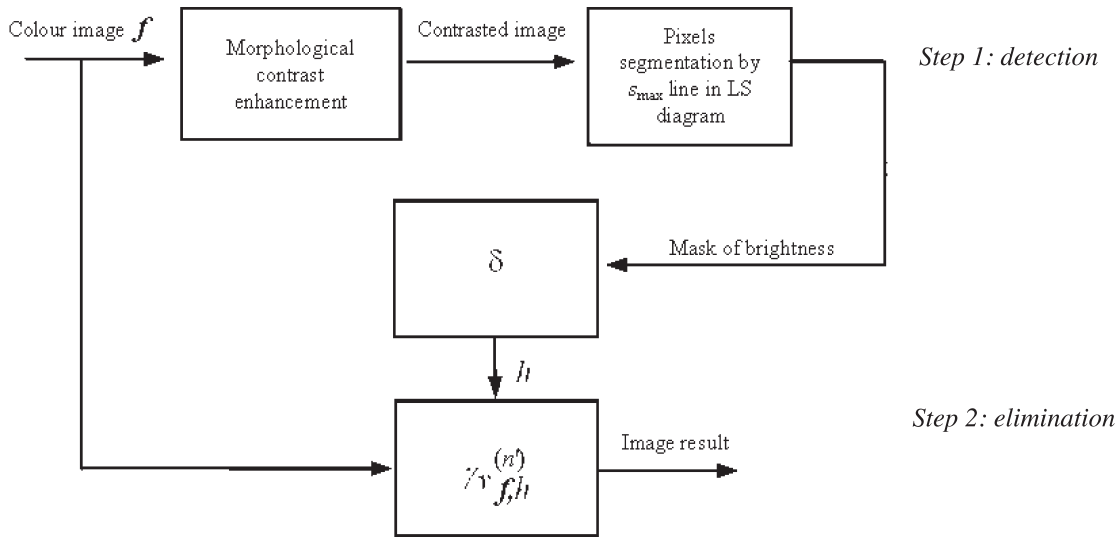

Figure 7. Algorithm steps for the detection and elimination of specular reflectance in color images.

The vectorial erosion of the opening by reconstruction is also done with a structural element of size e. This erosion replaces highlight pixels (high o_{lex}) by the surrounding chromatic pixels (low o_{lex}). Next, the vectorial geodesic dilation (iterated until stability) reconstructs the color image without the recovering the specularities. This is the same approach was successfully used in the detection of color cells in real-time medical imaging,[21] the filling in of holes[22] and Gaussian noise elimination in color images.[23]

With this new operation, we avoid some of the main inconveniences of the geodesic reconstruction, i.e., the high cost of processing caused by the multiple iterations of the reconstruction and the over-simplification of the image.[9] The main steps of the proposed method (and the precedence of the operations) are summarized in Fig. 7.

As can be seen in Fig. 7, the possibilities of parallel processing are very limited. Nevertheless, in order to achieve the results in a lower time, an alternative configuration for multiprocessor environment is possible, i.e., the vectorial erosion of the opening by reconstruction can be carried out in all the pixels of the original image $\boldsymbol{f}$ (in a second processor), in parallel with the detection step of the algorithm (first processor). This way, the first vectorial erosion (e = 1) of the top hat is reused. The task graph of this new configuration is shown in Fig. 8. We will evaluate this alternative in the following section.

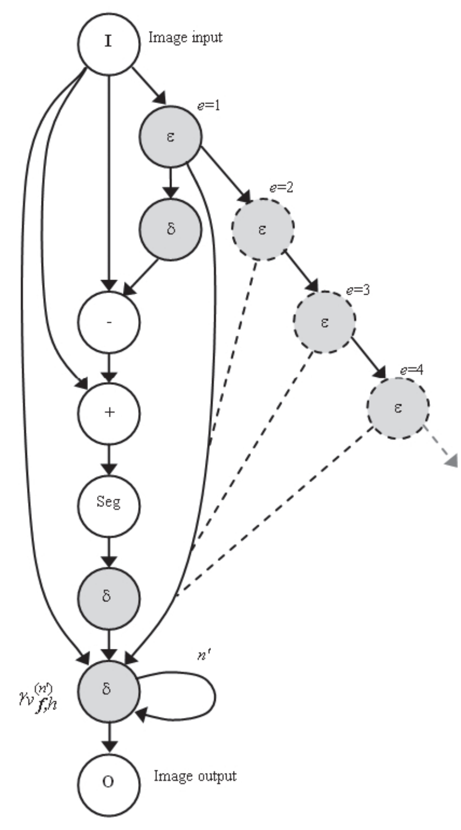

Figure 8. Task graph for a parallel processing of the algorithm. Morphological tasks in grey.

Experimental Results and Real-Time Aspects

We now present the results obtained from the application of our method for eliminating the specularities in the various real scenes shown in Fig. 3. In addition, we show a cost comparison for the two configurations of the algorithm: single processor and multi-processor.

The algorithms have operated mainly in a single 2.8 GHz standard processor PC system. Until now, the multiprocessor configuration has been only simulated using Visual software.[24] However, in order to exploit the parallel processing option in practice, we are now considering the execution of the algorithm over a multiprocessor system which consists of a standard mono-processor PC and a Matrox Genesis Board. This board has, in addition to a multi-channel frame grabber module, a low level image processor module. This last component is based on the TMS320C80 multi-processor and the Matrox NOA (Neighborhood Operation Accelerator) chip. With this multi-processor system, the morphological erosion is done on the genesis board, and the rest of operations are executed on the PC processor. In this way, we can achieve the parallelism described.

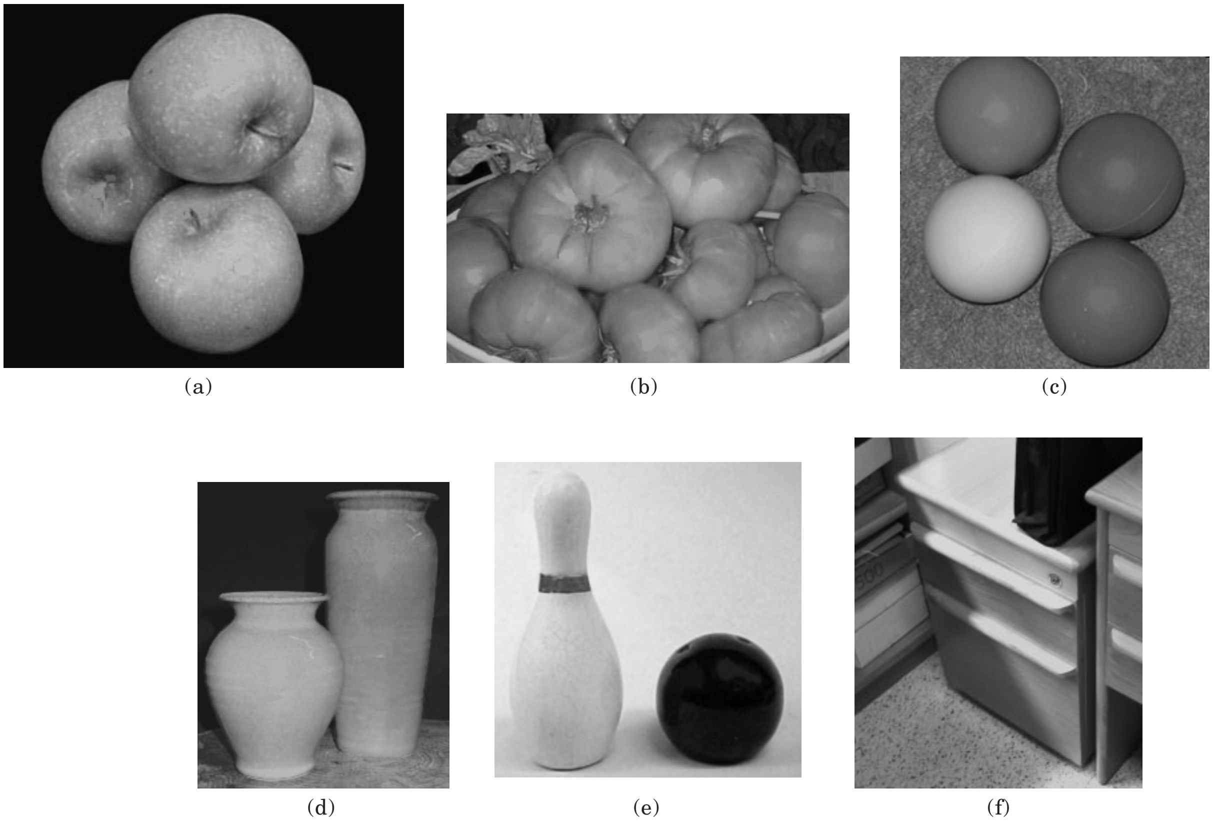

Figure 9. Elimination of specular reflectance of real color images in Fig. 3. Over-simplification is not present in the results. *Supplemental Material—Figure 9 can be found in color on the IS&T website (www.imaging.org) for a period of no less than two years from the date of publication.*

In Fig. 7, the main sequence of pseudo-code of the algorithm can be observed graphically. The complexities of the two configurations of the algorithm are similar, although the time of execution of the color algorithm in multi-processor descends because some color erosions are made in the second processor. The function "PixelsSegmentation" is the search for pixels in the chromatic image which have saturation and luminance corresponding to a vector of 25 values of coordinates (l,s) of $s_{\max}$ line. This way, only the pixels with specular reflectance and their neighborhoods are chosen for processing. The complexity associated to this function is determined by the search of these 25 values in the color image, i.e., 3 loops of size 25, N and M, being N and M the dimensions of the image. The last operations of the algorithm have the complexity of color morphological operations, i.e., $O(S \times V \times C)$, where S is the number of pixels in processing area (image h) and $S < N \times M$, V is the number of pixels in the neighborhood of structuring element e, and C is the number of color components.

From the visual results obtained (Fig. 9), the effectiveness of our method for the detection and elimination of specular reflectance can be observed. It must be emphasized that in the results obtained with the new filter, over-simplification does not appear since the reconstruction only functions in bright areas. Furthermore, the results are obtained at a much lower computational time which is compatible with real-time image processing systems.

The reconstruction task is the most critical operation. For this reason, the size e of the structuring element of morphological operations will depend on the application and real-time requirements, i.e., a low e (1,2) is recommended for visual inspection and a high e (3,4,...) is the best in multimedia and image restoration. An example of improvement in the results of the algorithm (for "balloons" image) according to the size of the structural element can be seen in Fig. 10. The CPU times (in seconds) for the two steps of the algorithm in single processing system are presented in Tables I and II.

TABLE I. CPU Times (seconds) for Step 1 of the Proposed Algorithm

Color image	Morphological contrast enhancement	Pixels segmentation by $s_{\max}$ line in LS
Apples	0.15	0.06
Tomatoes	0.12	0.05
Balloons	0.11	0.05
Vases	0.11	0.05
Bowling	0.11	0.05
Drawers	0.11	0.05

The speed of the PC's processor influences in the response times of the algorithms because the last operations of the algorithm (geodesic filter) are the ones that require more processing time, and they are always executed in the PC's processor (see Tables I and II). Executing some morphological erosions in a second processor (for example, Genesis board) decreases the total time, but the execution time of this operation is a lot shorter than the time required for the highlight elimi-

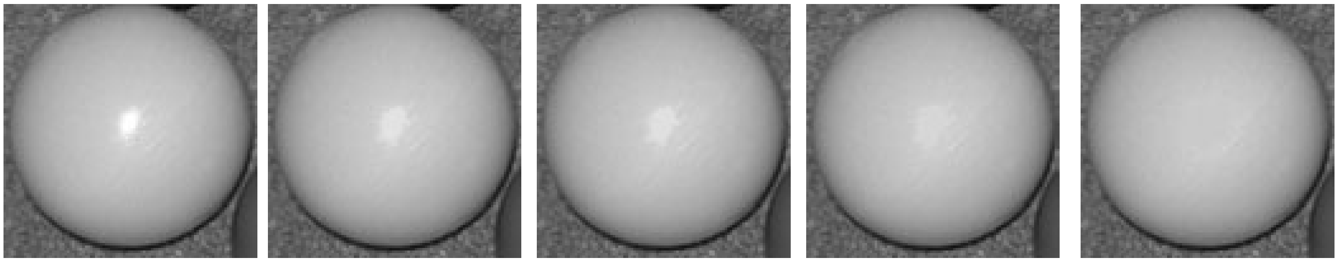

(a) (b) (c) (d) (e)

Figure 10. The improvement of brightness elimination by size of structuring element e in morphological operations. (a) Original image; (b) $e = 1$ (3×3); (c) $e = 2$ (5×5); (d) $e = 3$ (7×7); (e) $e = 4$ (9×9). *Supplemental Material—Figure 10 can be found in color on the IS&T website (www.imaging.org) for a period of no less than two years from the date of publication.*

TABLE II. CPU Times (seconds) for Step 2 of the Proposed Algorithm by Structuring Element of Size *e* in Morphological Operations. Single Processor Configuration

	Apples		Tomatoes		Balloons		Vases		Bowling		Drawers	
e	δ	$\gamma v^{(n')}_{\boldsymbol{f},h}$	δ	$\gamma v^{(n')}_{\boldsymbol{f},h}$	δ	$\gamma v^{(n')}_{\boldsymbol{f},h}$	δ	$\gamma v^{(n')}_{\boldsymbol{f},h}$	δ	$\gamma v^{(n')}_{\boldsymbol{f},h}$	δ	$\gamma v^{(n')}_{\boldsymbol{f},h}$
1	0.03	0.51	0.01	0.63	0.01	0.13	0.01	0.36	0.01	0.46	0.01	0.96
2	0.04	0.69	0.03	0.75	0.03	0.18	0.03	0.44	0.02	0.52	0.03	1.28
3	0.05	0.92	0.03	1.08	0.04	0.27	0.03	0.59	0.03	0.76	0.04	1.69
4	0.06	1.16	0.04	1.34	0.04	0.41	0.04	0.79	0.04	0.93	0.04	2.06

nation stage, and, thus, the speed of the second processor is not critical.

The multiprocessing allows us to reduce this CPU time between 0.07 seconds ($e = 1$) and 0.20 seconds ($e = 4$). This represents an additional reduction in temporal cost between 10% and 24%, with respect to a single processor configuration. In Table III, we show a comparison of temporal execution costs between the new algorithm for the elimination of specularities in color images and a global geodesic filter ($e = 1$) that operates over the entire image. As can be seen, the new method avoids the high computational cost of the geodesic processing for textured images ("Balloons" and "Drawers"), which is unacceptable for real-time requirements.

Finally, an evolution of times of execution (seconds) of the new algorithm according to the size of the structural element of the morphological operations is presented in Fig. 11.

Conclusions

In this article, we have presented a new method for the detection and elimination of specular reflectance in color images for real-time computer vision applications. The novelty of our investigation is the integration of the detection and the elimination of brightness in the same algorithm. In addition, all the operations for brightness elimination are based on color morphology.

A detailed study has demonstrated that the specularities in real scenes appear in a given area of the LS diagram, which is a 2D histogram of luminance and saturation signals. The use of a new connected vectorial filter allows us to eliminate the specular reflectance previously detected. This filter is an extension of the geodesic transformations of the mathematical morphology to color images. The possibility of eliminating highlights in color images without causing over-simplification has been demonstrated. In addition, the elimination of brightness has been obtained with a very low processing time, in single processor and multi-processor configurations, with respect to a global geodesic re-

TABLE III. Final CPU Times (seconds) for Brightness Elimination by Means of a Global Geodesic Filter, and the Proposed Algorithm for Single Processing and the Multiprocessing Configurations (*e* = 1)

Color image	Global filter	Proposed algorithm (Single-processing)	Proposed algorithm (Multiprocessing)
Apples	9.09	0.75	0.68
Tomatoes	11.73	0.81	0.73
Balloons	19.45	0.30	0.24
Vases	8.10	0.53	0.43
Bowling	8.64	0.63	0.57
Drawers	17.76	1.14	1.01

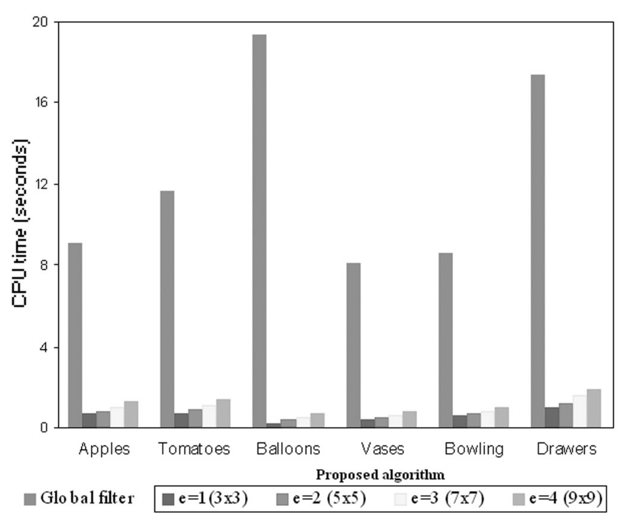

Figure 11. Evolution of execution times of the algorithm according to the size of the structural element of morphological operations. Multi-processor configuration of the algorithm with respect to the best time of single processor and global filter ($e = 1$).

construction. This permits us to achieve real-time requirements in image processing, even in very textured images. The detection and elimination of brightness is obtained independently of the material of the objects on which they appear, without any need of multiple view or previous knowledge of the scenes.

Based on the success shown by these results, we are working to improve our method for eliminating specularities. We work in other scheduling tasks and multi-processor configurations for color geodesic operations to reduce the processing time required in these operations as much as possible.

References

1. P. Laplante, *Real-Time Systems Design and Analysis*, 3rd ed., Wiley-IEEE Press, New-York, NY, 2003.
2. S. A. Shafer, Using color to separate reflection components, *Color Res. Appl.* **10,** 210, 1985.
3. S. Lin, Y. Li, S. Kang, X. Tong, and H. Shum, Diffuse-Specular Separation and Depth Recovery from Image Sequences, *Lecture Notes in Computer Science* **2352,** 210 (2002).
4. R. Bajcsy, S. Lee and A. Leonardis, Detection of diffuse and specular interface reflections and inter-reflections by color image segmentation, *Int'l. J. Computer Vision* **17,** 241 (1996).
5. G. Klinker, S. A. Shafer and T. Kanade, Image segmentation and reflection analysis through color, *Proc. SPIE* **937,** 229 (1988).
6. H. Palus, Representations of colour images in different colour spaces, in *The Colour Image Processing Handbook*, S. Sangwine, and R. Horne, Eds., Chapman and Hall, London, 1998, p. 67.
7. G. Wyszecki and W. S., Stiles, *Color Science, Concepts and Methods, Quantitative Data and Formulas*, 2nd ed., John Wiley, New York, NY, 1982.
8. K. N. Plataniotis and A. N. Venetsanopoulos, *Color Image Processing and Applications*, Springer-Verlag, Berlin, New York, 2000.
9. F. Ortiz, Procesamiento morfológico de imágenes en color. Aplicación a la reconstrucción geodésica, PhD Thesis, University of Alicante, Spain, 2002.
10. F. Torres, J. Angulo and F. Ortiz, Automatic detection of specular reflectance in colour images using the MS diagram, *Lecture Notes in Computer Science*, **2756,** 132 (2003).
11. J. Serra, *Image Analysis and Mathematical Morphology*, Vols. I and II, Academic Press, New York, NY, 1982 and 1988.
12. M. Comer and E. Delp, Morphological Operations for Color Image Processing, *J. Electronic Imaging* **8,** 279 (1999).
13. F. Ortiz, F. Torres, J. Angulo, and S. Puente, Comparative study of vectorial morphological operations in different color spaces, *Proc. SPIE* **4572,** 259 (2001).
14. A. Hanbury and J. Serra, Morphological operators on the unit circle, *IEEE Trans. Image Processing* **10,** 1842, 2001.
15. J. Angulo, Morphologie mathématique et indexation d'images couleur. Application à la microscopie en biomedicine, PhD Thesis, École des Mines de Paris, France, 2003.
16. L. Vicent, Morphological grayscale reconstruction in image analysis: Applications and efficient algorithms, *IEEE Trans. Image Processing* **2,** 176 (1993).
17. J. Crespo, J. Serra and R. Schafer, Theoretical aspects of morphological filters by reconstruction, *Signal Processing* **47,** 201, 1995.
18. P. Soille, *Morphological Image Analysis. Principles and Applications*, Springer-Verlag, Berlin, EU, 1999.
19. D. Androutsos, K. Plataniotis and A. Venetsanopoulos, A novel vector-based approach to color image retrieval using a vector angular-based distance measure, *Computer Vision and Image Understanding* **75,** 46 (1999).
20. P. Soille, A note on morphological contrast enhancement, *Technical Report RT-PS-001*, École des Mines d'Alès-EERIE, France, 1997.
21. F. Ortiz, F. Torres, E. De Juan, and N. Cuenca, Colour mathematical morphology for neural image analysis, *J. Real-Time Imaging* **8,** 455 (2002).
22. P. Soille and C. Gratin, An efficient algorithm for drainage networks extraction on DEMs, *J. Visual Comm. Image Represen.* **5,** 181 (1994).
23. F. Ortiz, F. Torres and P. Gil, Gaussian noise elimination in colour images by vector-connected filters, *Proc. IEEE 17th International Conference on Pattern Recognition*, vol. 4, IEEE Press, Los Alamitos, CA, 2004, p. 807.
24. F. Torres, F. Candelas, S. Puente, and F. Ortiz, Graph models applied to specification, simulation, allocation and scheduling of real-time computer vision applications, *J. Imaging Systems Technol.* **11,** 287 (2001).